














ARTICLE OPEN ACCESS

Physiologically Based Pharmacokinetic Model of Tyrosine Kinase Inhibitors to Predict Target Site Penetration, with PET-Guided Verification

Suzanne van der Gaag^{1,2}  | Tamara Jordens^{2,3}  | Maqsood Yaqub¹  | Robbin Grijseels³  |
 Daan W. van Valkengoed³  | Evelien N. de Langen³ | Ruben van den Broek³  | Victor L. J. L. Thijssen^{4,5,6}  |
 Adrianus J. de Langen⁷  | Mathilde C. M. Kouwenhoven^{8,9}  | Idris Bahce¹⁰  | Bart A. Westerman¹¹  |
 N. Harry Hendrikse^{1,2,12,13}  | Imke H. Bartelink^{2,3} 

¹Department of Radiology and Nuclear Medicine, Amsterdam UMC Location Vrije Universiteit Amsterdam, Amsterdam, the Netherlands | ²Cancer Center Amsterdam, Imaging and Biomarkers, Amsterdam, the Netherlands | ³Department of Clinical Pharmacology and Pharmacy, Amsterdam UMC Location Vrije Universiteit Amsterdam, Amsterdam, the Netherlands | ⁴Department of Radiation Oncology, Amsterdam UMC Location Vrije Universiteit Amsterdam, Amsterdam, the Netherlands | ⁵Center for Experimental and Molecular Medicine, Laboratory for Experimental Oncology and Radiobiology, Amsterdam UMC Location Amsterdam Medical Center, Amsterdam, the Netherlands | ⁶Cancer Center Amsterdam, Cancer Biology and Immunology, Amsterdam, the Netherlands | ⁷Department of Thoracic Oncology, The Netherlands Cancer Institute – Antoni van Leeuwenhoek Hospital, Amsterdam, the Netherlands | ⁸Department of Neurology, Amsterdam UMC Location Vrije Universiteit Amsterdam, Amsterdam, the Netherlands | ⁹Cancer Center Amsterdam, Brain Tumor Center Amsterdam, Amsterdam, the Netherlands | ¹⁰Department of Pulmonary Medicine, Amsterdam UMC Location Vrije Universiteit Amsterdam, Amsterdam, the Netherlands | ¹¹Department of Neurosurgery, Amsterdam UMC Location Vrije Universiteit Amsterdam, Amsterdam, the Netherlands | ¹²Department of Hospital Pharmacy, Erasmus MC, University Medical Center Rotterdam, Rotterdam, the Netherlands | ¹³Department of Radiology and Nuclear Medicine, Erasmus MC, University Medical Center Rotterdam, Rotterdam, the Netherlands

Correspondence: Imke H. Bartelink (i.bartelink@amsterdamumc.nl)

Received: 9 August 2024 | **Revised:** 10 January 2025 | **Accepted:** 15 January 2025

Funding: This research was supported by KWF Dutch Cancer Society grant 15486.

Keywords: epidermal growth factor receptor (EGFR) | non-small cell lung cancer (NSCLC) | physiologically based pharmacokinetic (PBPK) modeling | positron emission tomography (PET) | tyrosine kinase inhibitors (TKIs)

ABSTRACT

Osimertinib, a tyrosine kinase inhibitor (TKI), treats non-small cell lung cancer (NSCLC) with epidermal growth factor receptor (EGFR) mutations. However, its efficacy may vary due to heterogeneous drug distribution, assessable through microdosed radiolabeled drugs and positron emission tomography (PET). Precision dosing using microdosed TKI-PET encounters challenges due to pharmacokinetic (PK) variations between micro- and therapeutic doses. This study aims to predict osimertinib's tissue concentration–time profiles for both microdose and therapeutic dose scenarios using a whole-body physiologically based pharmacokinetic (PBPK) model, which incorporates nonlinear PK processes and target site occupancy. A target site PBPK model for osimertinib was developed to predict drug distribution across various tissues, including lung tumor, based on a previously published PBPK model. The model incorporated tissue-specific parameters and accounted for both linear and nonlinear pharmacokinetic processes, including EGFR-binding dynamics and tumor dynamics. Model predictions were verified with microdosed [¹¹C]-osimertinib PET imaging data and clinical pharmacokinetic profiles to assess accuracy and reliability. The developed target site-PBPK model accurately predicted osimertinib pharmacokinetics across multiple (tumor) tissues and dose levels within 2-fold error compared to observed PET data. This study underscores the utility of PBPK modeling in predicting osimertinib's

Suzanne van der Gaag and Tamara Jordens contributed equally to this work.

This is an open access article under the terms of the [Creative Commons Attribution-NonCommercial-NoDerivs](https://creativecommons.org/licenses/by-nc-nd/4.0/) License, which permits use and distribution in any medium, provided the original work is properly cited, the use is non-commercial and no modifications or adaptations are made.

© 2025 The Author(s). *CPT: Pharmacometrics & Systems Pharmacology* published by Wiley Periodicals LLC on behalf of American Society for Clinical Pharmacology and Therapeutics.

pharmacokinetics across diverse tissues, offering insights into drug distribution and predictions of target engagement in NSCLC patients using microdose PET imaging data. The developed model serves as a promising tool for optimizing dosing strategies and evaluating novel EGFR-TKIs in NSCLC treatment.

Summary

- What is the current knowledge on the topic?
 - Osimertinib, a third-generation EGFR-TKI, is used in NSCLC patients with EGFR mutations. Existing PBPK models can predict plasma drug concentrations but are often inadequate for predicting drug distribution in tissues, particularly in EGFR-rich compartments such as lung and tumors. These models typically do not account for EGFR-binding kinetics or tumor-specific dynamics.
- What question did this study address?
 - The study aimed to determine whether incorporating tumor-specific dynamics and nonlinear EGFR-binding kinetics into PBPK models could improve predictions of osimertinib distribution in target tissues. It also sought to validate the new target site-PBPK-model against patient data from microdose PET imaging ($[^{11}\text{C}]$ C-osimertinib) and therapeutic dosing.
- What does this study add to our knowledge?
 - This study improves PBPK models for osimertinib by incorporating tumor-specific dynamics and EGFR-binding kinetics, enabling more accurate predictions of drug distribution in EGFR-rich tissues like the lung and tumor. The model identified two distribution phases: a rapid decline postadministration and a slower phase driven by tissue distribution and EGFR binding. Validation using PET imaging and therapeutic dosing showed that most predictions were within acceptable error margins.
- How might this change drug discovery, development, and/or therapeutics?
 - This study enhances drug development with PBPK models that accurately predict tissue drug distribution, supporting targeted therapy evaluation. When appropriately validated, it may enable personalized dosing based on tumor size, EGFR expression, and patient variability. Microdose PET imaging based modeling in a limited number of patients reduces reliance on large clinical trials for predicting target attainment. Exploring tumor heterogeneity further refines predictions for individualized dosing strategies.

have emerged [2]. One of the most significant actionable driver mutations is the epidermal growth factor receptor (EGFR) mutation, occurring in approximately 10% of NSCLC cases in the Western population [3, 4]. Mutations within the EGFR kinase domain can result in constant, ligand-independent activation of the EGF receptor. Targeting these oncogenic pathways provides a promising approach, capable of reducing activated prosurvival signals, and increasing proapoptotic signals. Therefore, it holds significant interest in the treatment of cancers characterized by mutated EGFR [2, 4]. In approximately 85% of EGFR-mutated lung cancer patients, common mutations involving exon 19 deletion or L858R point mutation occur [5]. Tyrosine kinase inhibitors (TKIs), developed to specifically inhibit the EGFR signaling pathway, exhibit varying binding characteristics.

Despite initial success observed in clinical trials with early-generation EGFR-TKIs, drug resistance generally develops in less than a year [2, 6]. Acquired resistance is often attributed to the emergence of additional mutations, such as the EGFR T790M mutation [7]. T790M, in contrast to primary activating mutations like exon 19 deletion or exon 21 L858R, is an acquired resistance mutation that coexists with the original driver EGFR mutation. The discovery of this resistance mechanism prompted the development of third-generation EGFR-TKIs, such as osimertinib, primarily targeting T790M mutated EGFR. Osimertinib, with a 200-fold higher potency for inhibiting T790M mutated EGFR than wild-type EGFR [5, 8, 9], is currently the standard first-line therapy for all locally advanced and metastatic NSCLC patients harboring an activating EGFR mutation [9, 10].

Variability in drug distribution into tumor tissue can lead to sanctuary sites where some neoplastic cells receive insufficient TKI concentrations during treatment [11, 12]. Such variability of drug penetration into tumor tissues may result in suboptimal treatment responses [12]. Positron emission tomography (PET) with microdosed radioactively labeled drugs can be instrumental in identifying these sanctuary tumor sites and quantifying drug uptake at the site of action among patients [5, 13]. The resulting PET images offer valuable information for characterizing drug uptake at various tissues over time and their respective pharmacokinetic (PK) profiles. However, consideration is required when translating these PET image-based findings into the PK of therapeutic doses [14]. At therapeutic doses, enzymes involved in TKI binding and metabolism, drug-specific transporters, and EGFR-binding may become saturated, resulting in different metabolic patterns and tumor uptake compared with microdoses [15].

Physiologically based pharmacokinetic modeling (PBPK) is a modeling technique employed to predict the absorption, distribution, metabolism, and excretion (ADME) of drugs in humans. It combines system-specific parameters based on the physiology of different tissues and organs (e.g., volume, blood flow, pH, and

1 | Introduction

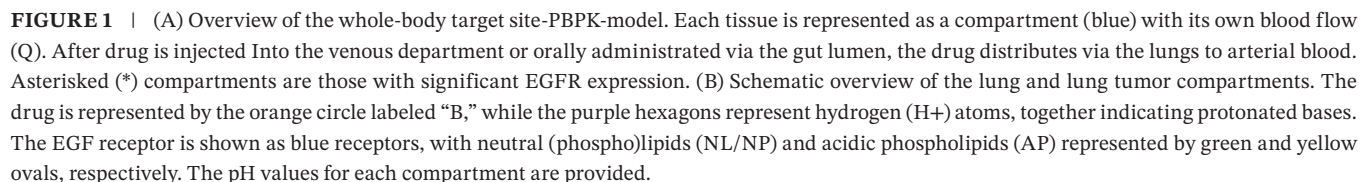
Lung cancer is the leading cause of cancer-related mortality worldwide [1]. Historically, non-small cell lung cancer (NSCLC), accounting for approximately 85% of all lung cancer diagnoses, has primarily been treated with cytotoxic chemotherapy. However, in recent years, novel targeted treatment modalities directed against specific oncogenic driver pathways

The current study therefore aimed to build a robust whole-body PBPK model for osimertinib mechanistically accounting for on- and off-target binding in all tissues, which allows exploration of the impact of EGFR binding on TKI PK. Accounting for these specific processes in a PBPK model allows us to generate deeper insights into target site-PK and is the first step in model-guided precision medicine for EGFR overexpressing Cancers. The model functionality was assessed based on microdosed PET imaging and therapeutic plasma PK data. Building upon the previous steady-state PBPK model [3], this comprehensive approach incorporated all known linear and nonlinear processes in drug absorption, distribution, metabolism, and elimination.

2.1 | Description of the Literature-Derived Whole Body PBPK Model (Base Model)

The model incorporated various compartments representing different tissues and organs: adipose, brain, gut, heart, kidney, liver, lung, lung tumor, muscle, pancreas, and spleen. A gut lumen compartment describes the absorption process of orally administered osimertinib [16]. Arterial and venous blood compartments capture the distribution and elimination processes [16]. The absorption, metabolism, and elimination rates of the drug were assumed to be linear across the entire dose range (Table S6 of Appendix S2). This assumption was based on the proportional increase in maximum plasma concentration (C_{\max}) and area under the curve (AUC) of osimertinib [19], similar with midazolam, a drug sharing a comparable metabolic profile [20] (Table S6).

For each tissue, tissue-to-plasma partition coefficients (K_p) were determined using the Rodgers and Rowland partition equations designed for moderate to strong bases (Appendix S4 and



visualized in Figure 1B) [21]. This calculation considered the transcellular distribution of the unprotonated drug and free fraction of the drug in plasma (F_u), as evaluated for the distribution of EGFR-TKI [3]. Osimertinib is a strong base with a pKa of 9.0 resulting in a high fraction of protonated drug at a physiological pH of 7.4 (0.975). Due to the protonated status in an environment with or below pH 7.4, the lysosomal sequestration or trapping (LYS) was added as previously described (Appendix S4, equation 5) [3, 22]. Here, the extravascular (EW) compartments consist of the sum of the remaining K_{pu} values and volumes (EW, NLNP, AP, and LYS) [3, 22].

2.2 | Target Site-PBPK: Adaptations to the Model

Two additions were made to the base model to better reflect the tumor and EGFR positive tissue distribution: (1) a tumor compartment was added, and (2) target site binding to EGFR was incorporated for all relevant tissues.

2.2.1 | Addition of the Tumor Compartment

A tumor compartment was added to the model as an additional compartment within the lung. Its flow, tissue density, and constitution were defined based on relevant literature data to enable accurate simulation of drug distribution. The tumor model included immune tumor deprivation (by reducing the cellular fraction of macrophages and type II cells); unaltered tumor perfusion compared with the surrounding lung tissue; and an acidic tumor environment (allowing a pH shift of the extracellular water of the tumor from 7.4 to 6.7). These NSCLC hallmarks have been described and verified previously by Bartelink et al. [3]. Spherical tumor volumes were calculated using the median baseline tumor diameters of 12 NSCLC lesions in four patients, and the tumor volume was established to be 3% of the entire lung volume [5]. Tumor cells can aggregate into a dense tumor mass, resulting in a cell density 1.7-fold higher than in healthy lung tissue, based on analyses of HE stains (Appendix S6). The higher cell density was incorporated into the model, using a virtual tumor volume (Table 1). Further details and all equations can be found in Appendix S4 and S5.

2.2.2 | EGFR Target Site Binding

EGFR binding was incorporated for tissues with significant EGFR expression (i.e., adipose, lung, lung tumor, kidney, heart, muscle, pancreas, skin, gut, and liver), using a nonlinear EGFR-binding model. The model incorporates the dynamics of extra and intracellular tissue binding. Due to osimertinib's physicochemical properties, including its strong basic nature and high lipophilicity (logD) interactions with (acidic phospho-) lipids drive the majority of the tissue distribution and leave only a small fraction available for target binding [3]. The interaction of osimertinib with EGFR takes place within the intracellular fluid of the cell, referred to in the model as intracellular water (IW). Osimertinib may bind to ATPase covalently in a 1:1 ratio [27]. Furthermore, only the fraction of the drug unbound to EGFR could freely return from the IW compartment to the

TABLE 1 | Tumor tissue, compound-specific input parameters.

Parameters	Value	Reference
EGFR (nM)	383	[23]
Mutation frequency in L858R/T790M Mutated NSCLC	50%	—
PH_{EW}	6.7	[24]
Tumor blood flow compared to lung (Q) ^a	3%	[24]
Virtual tumor volume ^b	5%	—
Cell density per gram	3×10^8	[25]
K_{on} WT EGFR ($nM^{-1} \cdot min^{-1}$)	0.174	[26]
K_{off} WT EGFR (min^{-1})	162	[26]
K_{on} L858R/T790M mutated EGFR ($nM^{-1} \cdot min^{-1}$)	0.186	[26]
K_{off} L858R/T790M mutated EGFR (min^{-1})	10.2	[26]
$K_{on,tumor}$ 50/50% WT/mutated ($nM^{-1} \cdot min^{-1}$)	0.18	[26]
$K_{off,tumor}$ 50/50% WT/mutated (min^{-1})	86.1	[26]

^aThe calculated tumor size based on tumor diameter was 3% of the lung, and tumor blood flow was assumed to be 3% the lung blood flow.

^bVirtual tumor volume is based on the tumor size compared to total lung volume and a factor correcting for the higher cell density of tumors compared to lung. Cell density in lung tumor tissue was estimated to be 1.7-fold higher than healthy lung tissue (Appendix S6).

EW compartment and subsequently re-enter the bloodstream (Figure 1B).

The binding prediction to osimertinib's target relies on in vitro-derived dissociation constants (K_D), derived from the association rate (K_{on}) and dissociation rate (K_{off}), of wild-type EGFR and activating EGFR mutations (Table 1) [28]. The K_D values are determined as a function of total concentrations in the in vitro system, including cells and proteins for stabilization. In the equation, $dA_{EGFRbound}$ represents the rate of change in the bound osimertinib with EGFR. The dynamics of this interaction are captured in Equation (1):

$$\frac{dA_{EGFRbound}}{dt} = \left(K_{on} * A_{tissue} * \left(\frac{EGFR_{tissue} * V_{tissue}}{V_{tissue_{IW}}} \right) \right) * fEGFR_{unbound} - K_{off} * A_{EGFR_{tissue}} \quad (1)$$

In the model the K_D of wild-type EGFR was used for all healthy tissues, whereas in tumor tissue, the K_D was split between 50% of cells with a K_D of wild-type EGFR and 50% with a K_D of L858R/T790M [27].

At therapeutic dose levels, EGFR may become saturated in tissues expressing the EGFR target [29]. To account for EGFR-binding saturation within the intracellular water, the fraction of unbound EGFR ($fEGFR_{unbound}$, Equation (2)), decreases as a function of both the amount of EGFR that has already bound

osimertinib and the total number of EGFR in each tissue (Figure 1B, Table 1; Appendix S5.2) [26].

$$f\text{EGFR}_{\text{unbound}} = 1 - \left(\frac{A_{\text{EGFR}_{\text{bound}}}}{A_{\text{EGFR}_{\text{tissue}}}} \right) \quad (2)$$

2.2.3 | Tissue EGFR Concentrations

Tissue EGFR concentrations were semi-quantified using a previously reported method based on immunohistochemistry (IHC) scores [30]. IHC scores from the human protein atlas (HPA) were linked to receptor density values (receptor/cell) reported by [30, 31]. These receptor densities were then converted into a total tissue concentration (nM) with Equation (3) with the assumption that 10^6 cells occupy $1 \mu\text{L}$ of tissue:

$$\text{EGFR}_{\text{total}} (\text{nM}) = \frac{\text{Receptors}}{\text{Cell}} * \frac{10^6 \text{ cells}}{\mu\text{L tissue}} * V_{\text{IW}} (\mu\text{L}) * \frac{1 \text{ mole}}{6.022 * 10^{23} \text{ receptors}} * \frac{1}{V_{\text{tissue}} (\text{L})} * 10^9 \quad (3)$$

For tissues with IHC scores of “Not Detected” according to the HPA (e.g., brain, spleen), EGFR concentrations were considered negligible and were excluded from the model.

2.3 | Model Verification

2.3.1 | Microdose PET Imaging Data

To ensure the accuracy and reliability, the developed target site-PBPK model was verified with actual patient data. Semi-quantification of PET-derived imaging data involved determining if there is a linear relationship between the arterial sampled whole blood PK and the standardized uptake value maximum (SUV_{max}) of the PET image of the descending aorta (Appendix S1, Figure S1). A significant correlation of 0.98 was identified. The study detailing patient information, tracer dose syntheses, blood PK-sampling, and both dynamic and static scans, has been previously described [5]. Briefly, patient enrollment involved obtaining written informed consent for participation in the approved study (CCMO number NL64722.031.18). Inclusion criteria involved patients experiencing disease progression on a first-generation EGFR-TKI with an activating mutation (EGFR exon 19 deletion or exon 21 L858R). A 2-week wash-out period was observed prior to the imaging.

Each patient underwent two imaging acquisitions; one while receiving 1 week of therapeutic dosing of TKI and one without. Following intravenous administration of a microdose [^{11}C]C-osimertinib (280 MBq, equivalent to $2.7 \mu\text{g}$), four patients were dynamically scanned twice, for 60 or 120 min within a 2-week window (the PET scan procedure is described in Appendix S7). Patients were not receiving osimertinib treatment prior to both scans. Each PET scan was accompanied by a low-dose computed tomography (CT) scan for attenuation and segmentation purposes. All PET image data underwent normalization, with corrections applied for dead-time, decay, randoms, scatter, and attenuation. Additional details regarding the scanning protocol, reconstructions, and simplified measures of uptake

(Standardized Uptake Value, SUV) from the scans are provided in the referenced publication [5].

Time-activity curves derived from the arterial and venous blood and dynamic PET images of the descending aorta, lung, and lung tumor were semi-quantified (Appendix S8) [5]. In addition to the dynamic scans, three of the four patients also underwent a whole-body static PET at 1 h after injection of [^{11}C]C-osimertinib. Time-activity curves for brain, kidney, liver, lung, spleen, and tumor at 60 min postinjection were semi-quantified based on tissue to blood ratios (TBR) (Appendix S8) [5]. A correction factor of 2.81 was employed to correct the SUV derived concentrations in the lung for the air fraction [32]. This factor allowed an adequate comparison of the PET observed with the target site-PBPK model predicted lung tissue density [32].

2.3.2 | Therapeutic PK data

To further evaluate the differences in microdose and therapeutic dose, predicted plasma concentration–time curves resulting from an orally administered 80 mg dose of osimertinib after a single dose and at steady-state were verified against the extracted PK profiles from healthy volunteers in the phase 1 study D5160C00001 [16]. Subjects in the Phase 1 study received a single 80 mg oral dose (7 days) of osimertinib followed by daily dosing for 22 days, and plasma samples were collected at various time points to construct concentration–time profiles. Furthermore, at steady state, target binding saturation was analyzed across all EGFR-expressing tissues to determine the extent of receptor occupancy.

2.3.3 | Statistics

The target site-PBPK model was verified using this empirical data (4 patients) by adjusting parameters to align simulated curves with observed profiles. This ensured the model accurately reflected osimertinib's pharmacokinetics at the therapeutic dose, confirming its reliability for predicting plasma concentrations across different dosing regimens and enhancing its utility for simulating clinical scenarios. The model's precision was considered adequate when the predicted plasma and tissue concentrations fell within 3-fold range of observed plasma and tissue concentrations derived from the microdosed patients or mean therapeutic PK data from literature. Despite general guidelines typically describing a 2-fold range, developments in model verification support the acceptance of a 3-fold range considering a small sample size and high inter- and inpatient variability in PK [24, 25, 33–35]. Observed plasma and tissue concentration of osimertinib were evaluated by calculating a prediction error (PE%) (Appendix S5.4) [36].

2.4 | Software

Model building was performed in R version 4.3.2 (2023-10-31 ucrt, <https://www.r-project.org/>) using the Rstudio development environment (version 2023.12.1) with the DeSolve package (version 1.40). Data transformation was conducted using the dplyr (version 1.1.4) and tidyverse (version 2.0.0)

packages. Therapeutic PK data was extracted from literature using WebPlotDigitizer version 4.6 (Ankit Rohatgi, <https://automeris.io/WebPlotDigitizer>).

3 | Results

3.1 | Base model and target site adaptations

The adaptations to the base model—addition of a tumor compartment and incorporation of EGFR target site binding—are demonstrated per tissue compartment in Appendix S9. These adaptations led to significant improvements in the accuracy of drug distribution predictions, particularly in the EGFR-rich compartments (lung and tumor, Appendix S10 bottom plots). At 60 min postadministration, the prediction error for all compartments fell within the acceptable 2-fold range, except for the liver (Table 2; Appendix S10). In contrast, the base model had

prediction errors exceeding threefold for the microdosed lung and tumor compartments, highlighting the significance of these adaptations for predicting target site PK, while the predictions of the therapeutic plasma PK was not significantly affected by the model adaptations (Appendix S10 top plots). The predictions for organs with EGFR expression, for which we obtained PET results, showed improvement.

3.2 | Model Verification

In total, four patients underwent two dynamic scans with [¹¹C]C-osimertinib. The two subsequent scans showed similar tumor and tissue uptake, irrespective of whether a first or second generation TKI was administered to steady-state (Figure 2), suggesting that no relevant saturation of pharmacokinetic processes can be observed using PET by comparing micro and steady-state TKI dosing. In the model verification,

TABLE 2 | Prediction errors of osimertinib in multiple tissues at 6 min and 1 h after microdose injection and 7 (corresponding with T_{max}) and 72 h (corresponding with ~2 times the half-life) after therapeutic dose, for the base model and the adapted EGFR model. Orange PEs indicate a >2-fold prediction error (67%), but within 3-fold prediction error (100%). Red PEs indicate a prediction error outside the 3-fold window.

Time postinjection (hours)	Dose	Tissue	PE base model (%)	PE EGFR model (%)	Contains EGFR
7	Therapeutic	Vein	20.1	17.4	No
72	Therapeutic	Vein	3.75	3.27	No
0.1	Micro	Vein	−8.55	−23.0	No
0.1	Micro	Artery	−9.00	12.5	No
0.1	Micro	Lung	−72.0	98.1	Yes
0.1	Micro	Tumor	−90.9	8.51	Yes
1	Micro	Lung	−175	−113	Yes
1	Micro	Brain	−16.7	−34.5	No
1	Micro	Kidney	−27.1	−6.21	Yes
1	Micro	Spleen	4.39	−8.06	No
1	Micro	Liver	−86.8	−71.8	Yes
1	Micro	Tumor	−142	−84.6	Yes

Abbreviation: PE, prediction error.

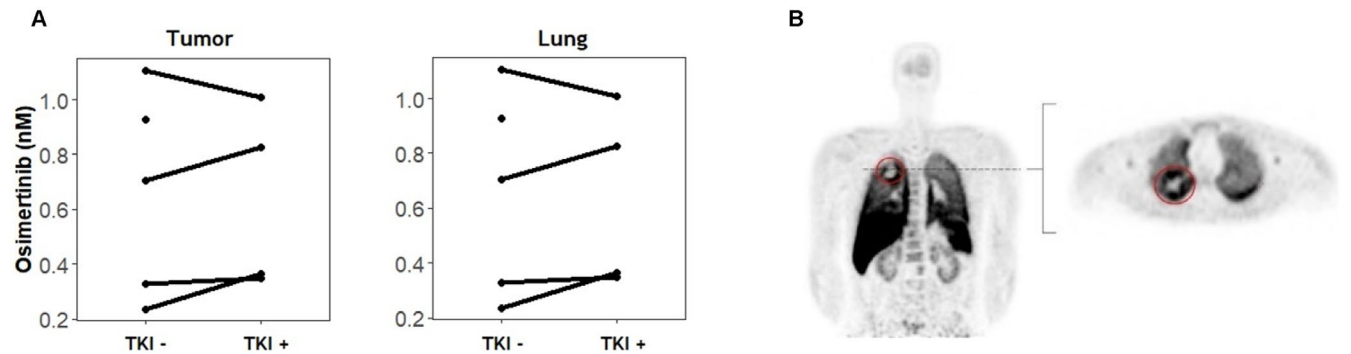


FIGURE 2 | (A) Results of [¹¹C]C-osimertinib dynamic scans in tumor and lung, differentiated by the presence (TKI+) or absence (TKI−) of a first or second generation TKI. (B) Representative PET/CT scan of a typical patient administered [¹¹C]C-osimertinib, with the tumor circled in red. Within the tumor, depicted as a black hot spot, a white area is observed, which may correspond to necrotic tumor tissue [5].

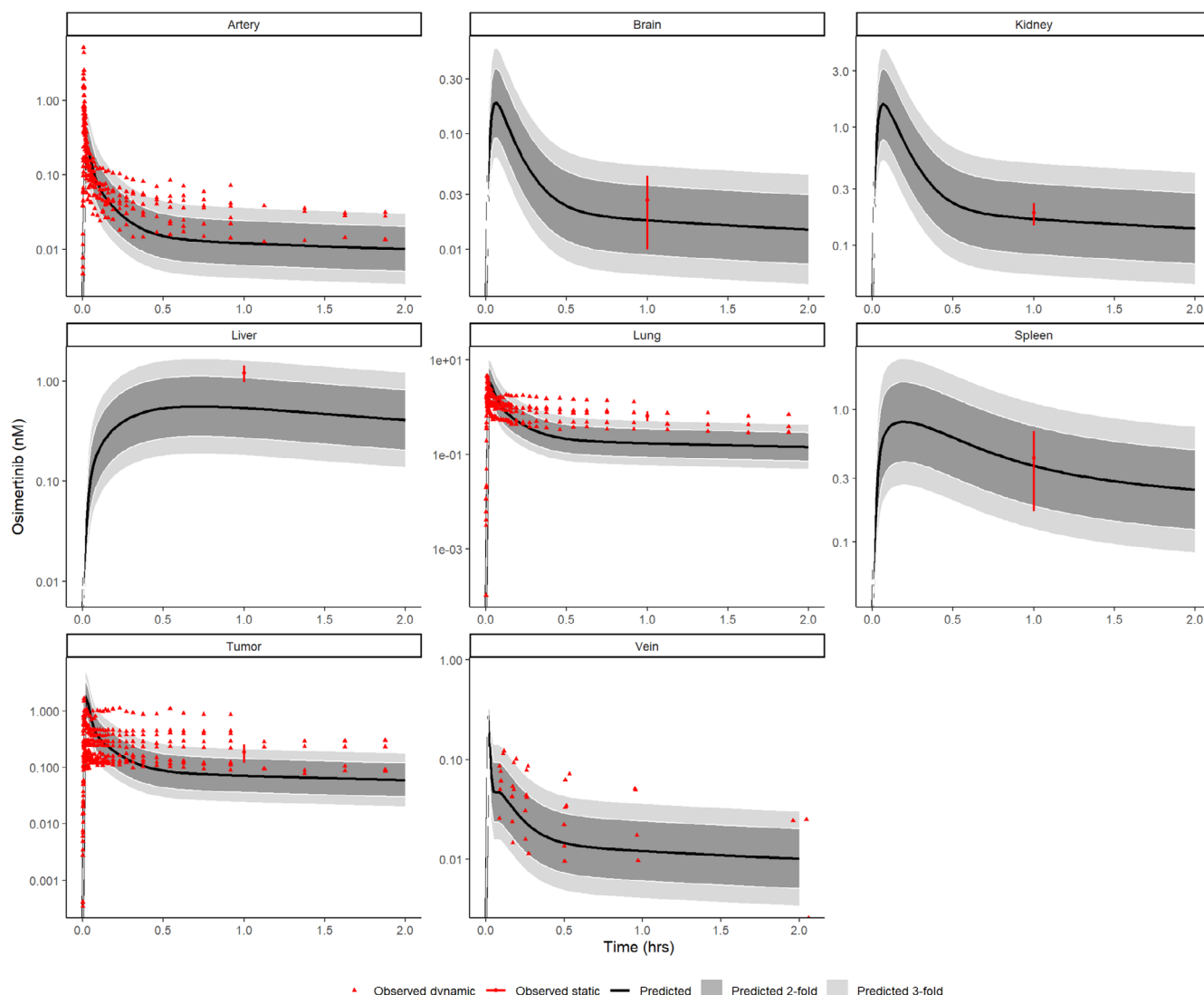


FIGURE 3 | Predicted osimertinib tissue concentrations (black lines), observed tissue concentrations after the whole body static PET scan ($n=3$) presented as mean with range (red circles) and after dynamic PET scan (red triangles) after a $2.7\mu\text{g}$ IV micro dose ($n=8$). A 2- and 3-fold range in predicted concentrations are depicted in dark gray and light gray, respectively.

data from both scans were pooled as concomitant therapeutic TKI administration did not influence the uptake of $[^{11}\text{C}]$ C-osimertinib.

3.2.1 | Model Predictions Versus Microdose Imaging Data

The model predicted the PK profiles of microdosed $[^{11}\text{C}]$ C-osimertinib in all tissues, maintaining predictions within a 3-fold margin (Figure 3, Table 2). Predicted concentrations were highest in the liver and spleen (0.538 and 0.347 nM, respectively) at 60 min postdose, while lowest in the brain and tumor (0.07 and 0.02 nM, respectively). This aligns with the PET image observations. Tumor-to-lung contrast was adequately predicted at all timepoints (PE tumor-to-lung ratio at 6 min of -91.4% and at 1 h 36.9%). Nonetheless, while both lung (98.1%) and tumor (8.51%) predictions after immediately after dosing are acceptable, the predicted concentrations for lung (-112%) after 60 min is outside the accepted 3-fold range.

3.2.2 | Model Predictions Versus Therapeutic PK Data

The model's prediction following the administration of an oral 80 mg dose of osimertinib indicates a predicted time to reach the maximum concentration in plasma (T_{max}) of 8.8 h, aligning with the (Figure 4A,B) observed T_{max} of 7 h [37]. The predicted $C_{\text{max,vein}}$ of 201 nM corresponds with the clinically observed $C_{\text{max,vein}}$ of 168 nM (PE of 45.5%, Table 2). The target site-PBPK model predicts half-life of osimertinib to be 52.4 h, which is longer than the observed half-life in studies involving NSCLC patients of 48 ± 2 h [38]. Since both half-lives are relatively long, defined as more than 24 h, and the predicted half-life falls within twofold of the observed half-life (8.76%) this discrepancy is deemed clinically insignificant. Nevertheless, the model effectively captures the concentrations up to 150 h following a single dose using Phase 1 data from NSCLC patients [16].

At steady state, the percentage of EGFR bound varies across tissues with a mean of 88% (SD = 5.9), reflecting differences in

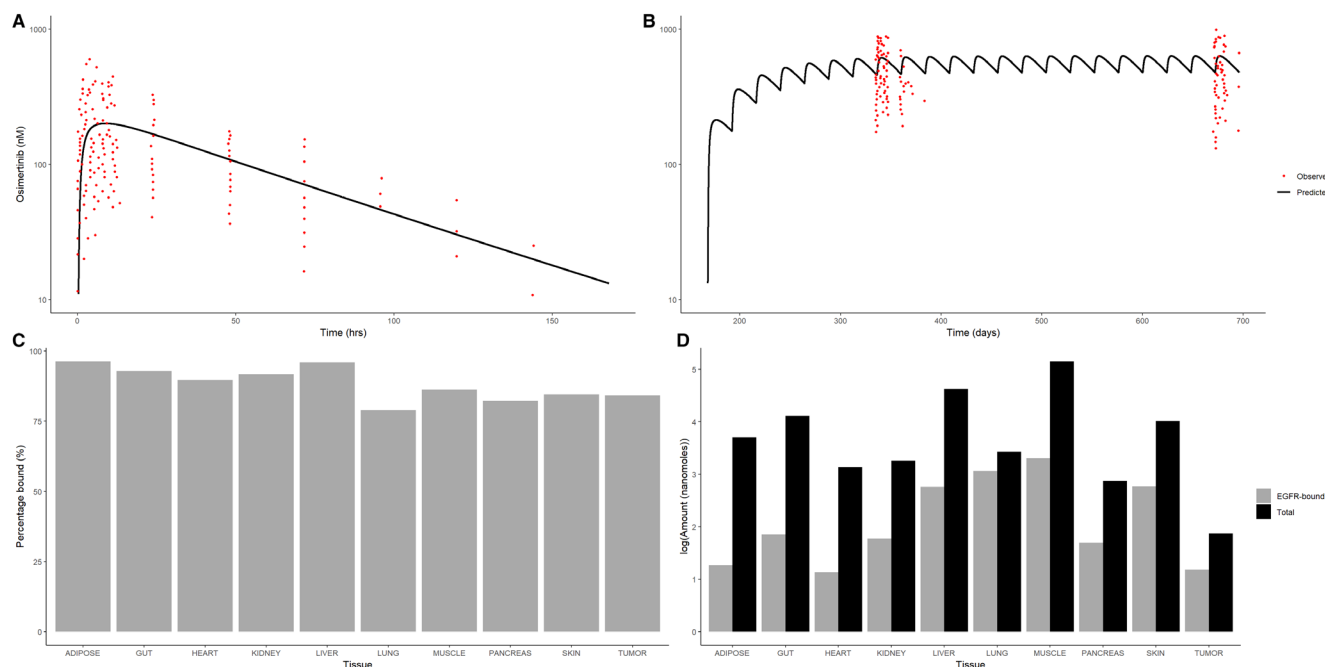


FIGURE 4 | Predicted profile (black) versus the observed concentration–time profiles of a group of 10 healthy volunteers receiving osimertinib (red) after (A) a single therapeutic 80mg oral dose and (B) at steady-state [19]. (C) Percentage of EGF receptor bound at therapeutic average steady-state concentration ($C_{ss,avg}$) for all EGFR-expressing organs. (D) Log-transformed total and EGFR-bound osimertinib amounts at therapeutic steady state in all EGFR-expressing organs.

EGFR saturation levels. These results show tissue-specific variability in target engagement (Figure 4C,D).

4 | Discussion

This study managed to improve the existing PBPK models of osimertinib PK as shown by verification with data from patients undergoing [^{11}C]C-osimertinib PET imaging in NSCLC patients and therapeutic plasma PK data in healthy volunteers. The target site-PBPK-model provided a comprehensive description of osimertinib concentrations in plasma and tissue, at both micro- and therapeutic dosages, achieved by expanding two previously published models and incorporating tumor dynamics and non-linear EGFR-binding kinetics [3, 29].

The new target site-PBPK model effectively predicted blood concentration at therapeutic doses by incorporating saturable EGFR binding, thereby improving accuracy of tissue PK predictions compared to models without EGFR binding. Microdose studies in lung and lung tumor tissue demonstrated a rapid drug distribution followed by a slower decline post-EGFR binding, a characteristic of third-generation TKIs (e.g., osimertinib) known for nonreversible EGFR binding and lower tumor K_{off} compared to wild type. Tissues showed two distribution phases: rapid decline after reaching C_{max} followed by a plateau, effectively modeled by segregating EGFR-expressing tissues into extracellular and EGFR-binding compartments. This approach, aligned with previous successes integrating receptor binding kinetics into PBPK models (e.g., PSMA ligand and high affinity drug targets such as bosentan), allows reliable prediction of PK profiles, emphasizing the extent of distribution [39, 40]. However, the new EGFR model did not significantly improve prediction errors in

the first minutes of drug distribution after bolus injection. This suggests that the distribution dynamics captured by the model at these early stages remain influenced by factors beyond the EGFR-specific binding and tumor adaptations, such as rapid blood tissue exchange or uncaptured initial drug distribution kinetics. Furthermore, the prediction error of the lung slightly exceeds the 3-fold error margin, potentially due to discrepancies between the in vitro data from the Human Protein Atlas and data derived from actual patients.

The new model explores factors influencing tumor uptake variability, particularly in relation to EGFR saturation. Simulations revealed tissue-specific differences in EGFR saturation at steady state, with all organs, including tumors, showing a target saturation of $> 75\%$ at 80 mg osimertinib once daily. Further exploration of variability between patients is a promising area for future research, ultimately aiming for dose individualization based on PBPK modeling.

The presented target site-PBPK model is to our knowledge the first of its kind in incorporating nonlinear target binding kinetics and NSCLC hallmarks in a whole body PBPK setting [41]. The model provides insights into osimertinib distribution in healthy and cancerous tissues after microdosing and therapeutic dosing. As our PET images allow macroscopic evaluation of drug distribution in a small number of patients, this research allowed assessment of EGFR target saturation on a population level. When quantifying the variability in EGFR saturation levels, these models may in future help to inform on personalized dosing strategies. Individual target site-PK predictions may suggest that for a patient with smaller EGFR-expressing tumors or limited EGFR density lower doses or dose frequencies could suffice, whereas those with larger tumors, greater EGFR expression or

other activating mutations may require higher doses to achieve adequate target engagement.

However, the binding affinity was derived from in vitro cellular experiments, not adjusting for the fraction unbound entering the intercellular water. This lack of adjustment may not necessarily reflect the actual k_{on} and k_{off} in all our patients. Future in vitro target association/dissociation experiments should focus on determining concentrations in each cellular fraction and measure actual target binding to EGFR.

Another study limitation is that although our target site-PBPK-model effectively predicted target attainment post multiple doses, it primarily focuses on single-dose plasma PK. To enhance predictions of steady-state concentrations, future iterations should integrate feedback mechanisms associated with EGFR binding, target inhibition, receptor internalization, and tumor growth modeling [42]. Despite accounting for NSCLC hallmarks like lysosomal sequestration, immune deprivation, and tumor microenvironment acidity, optimizing our model remains necessary, particularly to address the impact of tumor growth and drug effect during treatment.

Additionally, while the model brain prediction falls well within two-fold of observed concentrations at 60 min, the model currently assumes only passive diffusion across the blood–brain barrier (BBB). Colclough et al. [43] demonstrated in vitro in MDCK cells that osimertinib is a substrate for human BBB efflux transporters (MDR1 (P-gp)/BRCP) with an efflux ratio of 3.2, limiting the brain uptake of this drug. This is supported by osimertinib's unbound brain to unbound plasma ($K_{p_{uu}}$) ratio of 0.3 in rats [43], and its unbound cerebrospinal fluid to unbound plasma ratio of 0.16 in humans, indicating net efflux out of the central nervous system in vivo. 70% of NSCLC patients with EGFR mutations present with brain metastases during the course of the disease, indicating the relevance of considering BBB permeability of osimertinib [44, 45]. Furthermore, the ODIN-BM study showed expression in both healthy and brain metastasis tissue indicating that osimertinib readily crosses the BBB, although to different extents in various brain and brain tumor regions [46]. Hence, incorporating active transport mechanisms at the BBB and the blood–tumor–barrier (BTB) is crucial for refining brain permeability predictions over the entire time range. However, as the brain pertains only < 5% of the total quantity of the drug distribution, additional refinement is unlikely to impact the full body PK.

Moreover, considering osimertinib's extensive plasma protein binding to albumin of approximately 95%, which significantly prolongs its circulation time, our model focused solely on intrinsic unbound metabolic clearance, yet lacks information on active metabolite (AZ5104 & AZ7550) interactions with EGFR and albumin, critical for predicting steady-state drug levels [47].

To enable the application of target site model-based TKI dosing, future research should focus on quantifying heterogeneity of osimertinib target site concentrations, both within individual tumors and across patients, at a microscopic and cellular scale. This requires integrating individual PET image results with EGFR expression data obtained from tumor biopsies to better characterize inter- and intraindividual variability in EGFR

density. Additionally, microscopic PK-assessment techniques (e.g., MALDI-MSI) could be employed to visualize whether the drug distributes homogeneously throughout the tumor (biopsy) and effectively engages all target receptors [12]. Expanding of the current model to identify sanctuary tumor sites and incorporate spatial information on drug distribution is essential. More advanced estimation methods, such as nonlinear mixed effect modeling (NONMEM), can be utilized to predict PK heterogeneity and optimize personalized dosing strategies.

Our findings highlight the limitations of current models and emphasize the potential value of incorporating EGFR heterogeneity to improve predictions of osimertinib distribution and target engagement. Inter- and intraindividual variations in EGFR density among patients and tumor influence drug accumulation in the tumor. Conducting a sensitivity analysis can evaluate how these variables impact drug predictions. Quantifying EGFR density via histology alongside drug uptake measurements could enhance predictive models and may enable dose predictions for achieving full target attainment.

5 | Conclusion

In conclusion, this study demonstrates the potential of the mechanistic PBPK modeling approach to generate predictions of osimertinib distribution across various tissues, within a reasonable margin of error. By simulating both microdose and therapeutic dose scenarios, the model facilitates the exploration of systemic osimertinib pharmacokinetics. While promising for understanding concentrations in on- and off-target tissues, this target site-PBPK model is primarily intended for hypothesis generation due to limited available data. Future clinical PK studies are planned to further validate the model. With the inclusion of diverse drug-specific parameters, the new model may also be used to predict target-tissue concentrations over time and evaluate the viability of novel EGFR-TKIs.

Author Contributions

S.G., T.J., and I.H.B. wrote the manuscript. S.G., T.J., M.Y., V.L.J.L.T., A.J.L., M.C.M.K., I.B., B.A.W., N.H.H., and I.H.B. designed the research. S.G., T.J., R.G., D.W.V., E.N.L., R.B., and I.H.B. performed the research. S.G., T.J., R.G., D.W.V., E.N.L., R.B., and I.H.B. analyzed the data.

Acknowledgments

We extend our gratitude to Zahra Ahmadian and Eline Beers for their invaluable contributions to the modeling work presented in this manuscript and Michael Cloesmeijer and Olivier Béquignon for their input in the mechanistical model development.

Conflicts of Interest

We disclose that Dr. I. Bahce occasionally participates in advisory boards for Boehringer Ingelheim, with no additional conflicts of interest to disclose. All other authors declared no competing interests for this work.

Data Availability Statement

The data generated in this study are available within the article and its supplementary data files. Additional data are available upon reasonable

request from the corresponding author. The model that support the findings of this study are openly available on GitHub at <https://github.com/ibartelink/Target-Site-PBPK-in-oncology.git>. This includes instructions on how to run the model and obtain results.

References

1. R. L. Siegel, K. D. Miller, H. E. Fuchs, and A. Jemal, "Cancer Statistics, 2022," *CA: A Cancer Journal for Clinicians* 72, no. 1 (2022): 7–33.
2. M. Faehling, B. Schwenk, S. Kramberg, et al., "Oncogenic Driver Mutations, Treatment, and EGFR-TKI Resistance in a Caucasian Population with Non-Small Cell Lung Cancer: Survival in Clinical Practice," *Oncotarget* 8, no. 44 (2017): 77897–77914.
3. I. H. Bartelink, E. A. van de Stadt, A. F. Leeuwerik, et al., "Physiologically Based Pharmacokinetic (PBPK) Modeling to Predict PET Image Quality of Three Generations EGFR TKI in Advanced-Stage NSCLC Patients," *Pharmaceuticals* 15, no. 7 (2022): 796.
4. T. Hirano, H. Yasuda, T. Tani, et al., "In Vitro Modeling to Determine Mutation Specificity of EGFR Tyrosine Kinase Inhibitors Against Clinically Relevant EGFR Mutants in Non-Small-Cell Lung Cancer," *Oncotarget* 6, no. 36 (2015): 38789–38803.
5. E. A. van de Stadt, M. Yaqub, R. C. Schuit, et al., "Relationship Between Biodistribution and Tracer Kinetics of ^{11}C -Erlotinib, ^{18}F -Afatinib and ^{11}C -Osimertinib and Image Quality Evaluation Using Pharmacokinetic/Pharmacodynamic Analysis in Advanced Stage Non-Small Cell Lung Cancer Patients," *Diagnostics* 12, no. 4 (2022): 883.
6. M. J. Eck and C. H. Yun, "Structural and Mechanistic Underpinnings of the Differential Drug Sensitivity of EGFR Mutations in Non-Small Cell Lung Cancer," *Biochimica et Biophysica Acta* 1804, no. 3 (2010): 559–566.
7. C. H. Yun, K. E. Mengwasser, A. V. Toms, et al., "The T790M Mutation in EGFR Kinase Causes Drug Resistance by Increasing the Affinity for ATP," *Proceedings of the National Academy of Sciences of the United States of America* 105, no. 6 (2008): 2070–2075.
8. S. Klaeger, S. Heinzlmeir, M. Wilhelm, et al., "The Target Landscape of Clinical Kinase Drugs," *Science* 358, no. 6367 (2017): eaan4368.
9. J. C. Soria, Y. Ohe, J. Vansteenkiste, et al., "Osimertinib in Untreated EGFR-Mutated Advanced Non-Small-Cell Lung Cancer," *New England Journal of Medicine* 378, no. 2 (2018): 113–125.
10. V. Ernani and T. E. Stinchcombe, "Management of Brain Metastases in Non-Small-Cell Lung Cancer," *Journal of Oncology Practice/American Society of Clinical Oncology* 15, no. 11 (2019): 563–570.
11. I. H. Bartelink, B. Prideaux, G. Krings, et al., "Heterogeneous Drug Penetration of Veliparib and Carboplatin Measured in Triple Negative Breast Tumors," *Breast Cancer Research* 19, no. 1 (2017): 107.
12. I. H. Bartelink, E. F. Jones, S. K. Shahidi-Latham, et al., "Tumor Drug Penetration Measurements Could Be the Neglected Piece of the Personalized Cancer Treatment Puzzle," *Clinical Pharmacology and Therapeutics* 106, no. 1 (2019): 148–163.
13. A. Varrone, K. Varnäs, A. Jucaite, et al., "A PET Study in Healthy Subjects of Brain Exposure of ^{11}C -Labelled Osimertinib – A Drug Intended for Treatment of Brain Metastases in Non-Small Cell Lung Cancer," *Journal of Cerebral Blood Flow and Metabolism* 40, no. 4 (2020): 799–807.
14. T. Burt, K. Yoshida, G. Lappin, et al., "Microdosing and Other Phase 0 Clinical Trials: Facilitating Translation in Drug Development," *Clinical and Translational Science* 9, no. 2 (2016): 74–88.
15. I. Bahce, E. F. Smit, M. Lubberink, et al., "Development of [^{11}C]erlotinib Positron Emission Tomography for In Vivo Evaluation of EGF Receptor Mutational Status," *Clinical Cancer Research* 19, no. 1 (2013): 183–193.
16. V. P. Reddy, M. Walker, P. Sharma, P. Ballard, and K. Vishwanathan, "Development, Verification, and Prediction of Osimertinib Drug-Drug Interactions Using PBPK Modeling Approach to Inform Drug Label," *CPT: Pharmacometrics & Systems Pharmacology* 9, no. 5 (2018): 321–330.
17. T. Rodgers and M. Rowland, "Physiologically Based Pharmacokinetic Modelling 2: Predicting the Tissue Distribution of Acids, Very Weak Bases, Neutrals and Zwitterions," *Journal of Pharmaceutical Sciences* 95, no. 6 (2006): 1238–1257.
18. H. M. Jones, N. Parrott, K. Jorga, and T. Lavé, "A Novel Strategy for Physiologically Based Predictions of Human Pharmacokinetics," *Clinical Pharmacokinetics* 45, no. 5 (2006): 511–542.
19. M. Santarpia, A. Ligouri, N. Karachaliou, et al., "Osimertinib in the Treatment of Non-Small-Cell Lung Cancer: Design, Development and Place in Therapy," *Lung Cancer* 8 (2017): 109–125.
20. G. Lappin, W. Kuhn, R. Jochemsen, et al., "Use of Microdosing to Predict Pharmacokinetics at the Therapeutic Dose: Experience with 5 Drugs," *Clinical Pharmacology and Therapeutics* 80, no. 3 (2006): 203–215.
21. T. Rodgers, D. Leahy, and M. Rowland, "Physiologically Based Pharmacokinetic Modeling 1: Predicting the Tissue Distribution of Moderate-to-Strong Bases," *Journal of Pharmaceutical Sciences* 94, no. 6 (2005): 1259–1276.
22. M. V. Schmitt, R. Reichel, X. Liu, G. Fricker, and P. Lienau, "Extension of the Mechanistic Tissue Distribution Model of Rodgers and Rowland by Systemic Incorporation of Lysosomal Trapping: Impact on Unbound Partition Coefficient and Volume of Distribution Predictions in the Rat," *Drug Metabolism and Disposition* 49, no. 1 (2021): 53–61.
23. U. Del Monte, "Does the Cell Number 10(9) Still Really Fit One Gram of Tumor Tissue?," *Cell Cycle* 8, no. 3 (2009): 505–506.
24. Administration USFaD, "Guidance for Industry: Physiologically Based Pharmacokinetic Analyses—Format and Content." (2016).
25. M. Shebley, P. Sandu, A. Riedmaier, et al., "Physiologically Based Pharmacokinetic Model Qualification and Reporting Procedures for Regulatory Submissions: A Consortium Perspective," *Clinical Pharmacology and Therapeutics* 104, no. 1 (2018): 88–110.
26. T. Ren, X. Zhu, N. M. Jusko, W. Krzyzanski, and W. J. Jusko, "Pharmacodynamic Model of Slow Reversible Binding and its Applications in Pharmacokinetic/Pharmacodynamic Modeling: Review and Tutorial," *Journal of Pharmacokinetics and Pharmacodynamics* 49, no. 5 (2022): 493–510.
27. T. S. Beyett, C. To, D. E. Heppner, et al., "Molecular Basis for Cooperative Binding and Synergy of ATP-Site and Allosteric EGFR Inhibitors," *Nature Communications* 13, no. 1 (2022): 2530.
28. X. Zhai, R. A. Ward, P. Doig, and A. Argyrou, "Insight into the Therapeutic Selectivity of the Irreversible EGFR Tyrosine Kinase Inhibitor Osimertinib through Enzyme Kinetic Studies," *Biochemistry* 59, no. 14 (2020): 1428–1441.
29. A. Haouala, N. Widmer, M. Guidi, et al., "Prediction of Free Imatinib Concentrations Based on Total Plasma Concentrations in Patients with Gastrointestinal Stromal Tumours," *British Journal of Clinical Pharmacology* 75, no. 4 (2013): 1007–1018.
30. P. M. Glassman and J. P. Balthasar, "Physiologically-Based Pharmacokinetic Modeling to Predict the Clinical Pharmacokinetics of Monoclonal Antibodies," *Journal of Pharmacokinetics and Pharmacodynamics* 43, no. 4 (2016): 427–446.
31. M. Uhlen, C. Zhang, S. Lee, et al., "A Pathology Atlas of the Human Cancer Transcriptome," *Science* 357, no. 6352 (2017): eaan2507.
32. T. Lambrou, A. M. Groves, K. Erlandsson, et al., "The Importance of Correction for Tissue Fraction Effects in Lung PET: Preliminary Findings," *European Journal of Nuclear Medicine and Molecular Imaging* 38, no. 12 (2011): 2238–2246.
33. Agency EM, "Guideline on the Qualification and Reporting of Physiologically Based Pharmacokinetic (PBPK) Modelling and Simulation," 2016.

34. K. Abduljalil, T. Cain, H. Humphries, and A. Rostami-Hodjegan, "Deciding on Success Criteria for Predictability of Pharmacokinetic Parameters from In Vitro Studies: An Analysis Based on In Vivo Observations," *Drug Metabolism and Disposition* 42, no. 9 (2014): 1478–1484.
35. N. Isoherranen, "How Should a PBPK Model Be Evaluated for Intended Use?," *Drug Metabolism and Pharmacokinetics* 33, no. 1 (2018): S8.
36. G. Wu, M. Baraldo, and M. Furlanut, "Calculating Percentage Prediction Error: A User's Note," *Pharmacological Research* 32, no. 4 (1995): 241–248.
37. K. Vishwanathan, K. So, K. Thomas, A. Bramley, S. Englisg, and J. Collier, "Absolute Bioavailability of Osimertinib in Healthy Adults," *Clinical Pharmacology in Drug Development* 8, no. 2 (2019): 198–207.
38. K. Brown, C. Comisar, H. Witjes, et al., "Population Pharmacokinetics and Exposure-Response of Osimertinib in Patients with Non-Small Cell Lung Cancer," *British Journal of Clinical Pharmacology* 83, no. 6 (2017): 1216–1226.
39. S. Koyama, K. Toshimoto, W. Lee, Y. Aoki, and Y. Sugiyama, "Revisiting Nonlinear Bosentan Pharmacokinetics by Physiologically Based Pharmacokinetic Modeling: Target Binding, Albeit Not a Major Contributor to Nonlinearity, Can Offer Prediction of Target Occupancy," *Drug Metabolism and Disposition* 49, no. 4 (2021): 298–304.
40. N. J. Begum, G. Glatting, H. J. Wester, M. Eiber, A. J. Beer, and P. Kletting, "The Effect of Ligand Amount, Affinity and Internalization on PSMA-Targeted Imaging and Therapy: A Simulation Study Using a PBPK Model," *Scientific Reports* 9, no. 1 (2019): 20041.
41. F. Liang, Y. Zhang, Q. Xue, and X. Zhang, "Integrated PBPK-EO Modeling of Osimertinib to Predict Plasma Concentrations and Intracranial EGFR Engagement in Patient with Brain Metastases," *Scientific Reports* 14, no. 1 (2024): 12736.
42. A. Sorkin and J. E. Duex, "Quantitative Analysis of Endocytosis and Turnover of Epidermal Growth Factor (EGF) and EGF Receptor," *Current Protocols in Cell Biology* 15 (2010): Unit 15.14.
43. N. Colclough, K. Chen, P. Johnström, et al., "Preclinical Comparison of the Blood-Brain Barrier Permeability of Osimertinib With Other EGFR TKIs," *Clinical Cancer Research* 27, no. 1 (2021): 189–201.
44. J. C. Yang, B. C. Cho, D. W. Kim, et al., "Osimertinib for Patients with Leptomeningeal Metastases from EGFR-Mutant Non-Small Cell Lung Cancer: Updated Results from the BLOOM-Study," *Journal of Clinical Oncology* 35, no. 15 (2017): 2020.
45. J. J. A. O. Schoenmaekers, S. Dursun, C. Biesmans, et al., "Dynamics of Eligibility Criteria For Central Nervous System Metastases in Non-Small Cell Lung Cancer Randomized Clinical Trials Over Time: A Systemic Review," *Critical Reviews in Oncology/Hematology* 166 (2021): 103460.
46. S. Ekman, Z. Cselényi, A. Varrone, et al., "Brain Exposure of Osimertinib in Patients With Epidermal Growth Factor Receptor Mutation Non-Small Cell Lung Cancer and Brain Metastases: A Positron Emission Tomography and Magnetic Resonance Imaging Study," *Clinical and Translational Science* 16, no. 6 (2023): 955–965.
47. Y. Wu, L. Chen, J. Chen, et al., "Covalent Binding Mechanism of Furmonertinib and Osimertinib With Human Serum Albumin," *Drug Metabolism and Disposition* 51, no. 1 (2023): 8–16.

Supporting Information

Additional supporting information can be found online in the Supporting Information section.